

# Intercalation and Delamination of Layered Carbides (MXenes)

Olha Mashtalir,<sup>1,2</sup> Michael Naguib,<sup>1,2</sup> Vadym N. Mochalin,<sup>1,2</sup> Yohan Dall'Agnese,<sup>1,2</sup> Min Heon,<sup>1,2</sup>

Michel W. Barsoum<sup>1\*</sup> and Yury Gogotsi<sup>1,2\*</sup>

Intercalation and delamination of two-dimensional (2D) solids in many cases is a requisite step for exploiting their unique properties. Herein we report on the intercalation of 2D,  $Ti_3C_2$ ,  $Ti_3CN$  and  $TiNbC$  – so called MXenes - materials. Intercalation of hydrazine, and its co-intercalation with DMF, resulted in an increase of the  $c$  lattice parameter of  $Ti_3C_2$  from 19.5 Å to 25.48 Å and 26.80 Å, respectively. Urea also intercalated  $Ti_3C_2$ . Molecular dynamics simulations suggest that a hydrazine monolayer intercalates between the  $Ti_3C_2$  layers. Hydrazine also intercalated  $Ti_3CN$  and  $TiNbC$ . When dimethyl sulfoxide was intercalated into  $Ti_3C_2$ , followed by sonication in water, it delaminated forming a stable colloidal solution that was in turn filtered to produce MXene paper. The latter showed excellent Li ion capacity at extremely high charging rates.

---

<sup>1</sup> Department of Materials Science and Engineering & <sup>2</sup> A.J. Drexel Nanotechnology Institute, Drexel University, 3141 Chestnut St., Philadelphia, PA 19104, USA. \* E-mail: [gogotsi@drexel.edu](mailto:gogotsi@drexel.edu); [barsoumw@drexel.edu](mailto:barsoumw@drexel.edu)

A unique characteristic of layered materials is their ability to accommodate various ions and molecules between their layers, a phenomenon known as intercalation. Intercalation compounds of inorganic hosts (graphite<sup>1</sup>, clays, di-chalcogenides and others) have also gained renewed interest due to their unique chemical and physical properties<sup>2-6</sup>. De-intercalation of those compounds under certain conditions (e.g., thermal shock, sonication or volume expansion reactions in the interlayer space) leads to formation of widely used exfoliated graphite<sup>7-11</sup> and two-dimensional (2D) materials with unusual electronic properties<sup>12-15</sup>.

Recently, a large family of 2D materials, labeled MXenes - produced by the extraction of the A-element from the layered ternary carbides (e.g.,  $\text{Ti}_3\text{AlC}_2$ ) known as MAX phases<sup>16</sup>, where M is an early transition metal, A is an A group element and X is C or N - was discovered<sup>17, 18</sup>. The MXenes produced to date, viz.  $\text{Ti}_3\text{C}_2$ <sup>17</sup>,  $\text{Ti}_2\text{C}$ ,  $\text{Ta}_4\text{C}_3$ ,  $(\text{Ti}_{0.5}\text{Nb}_{0.5})_2\text{C}$ ,  $(\text{V}_{0.5}\text{Cr}_{0.5})_3\text{C}_2$ ,  $\text{Ti}_3\text{CN}$ <sup>18</sup> are, in many aspects, graphene-like, forming stacks of sheets and scrolls. They also are good electrical conductors<sup>17-21</sup>. Electrochemical intercalation of Li ions between  $\text{Ti}_3\text{C}_2$  sheets renders these solids promising materials for Li-ion battery anodes and hybrid electrochemical capacitors<sup>22-24</sup>. However, there are currently no reports of the chemical intercalation or large-scale delamination of MXenes or other transition metal carbides.

It is important to note that the 2D  $\text{Ti}_3\text{C}_2$  surfaces are *not* Ti-terminated, but covered with oxygen-containing groups (e.g., OH) and fluorine, F, left over after HF etching<sup>17</sup>. For brevity's sake, MXene or  $\text{Ti}_3\text{C}_2$  will be used instead of the more cumbersome  $\text{Ti}_3\text{C}_2(\text{OH})_x\text{O}_y\text{F}_z$ . The original aim of this work was to reduce the  $\text{Ti}_3\text{C}_2$  surfaces to create Ti-terminated surfaces that theory predicts would be magnetic<sup>24</sup>. A perusal of the graphene literature made it amply clear that hydrazine monohydrate  $\text{N}_2\text{H}_4 \cdot \text{H}_2\text{O}$  (HM) dissolved in N,N-dimethylformamide (DMF) is the reactant of choice<sup>25</sup>. Furthermore, since MXenes can be thought of as conductive clays<sup>17</sup>, we reviewed the

intercalation chemistries of the latter. Numerous compounds, such as formamide and its derivatives, dimethyl sulfoxide (DMSO), urea, long-chain alkylamines, and others, have been shown to intercalate clays<sup>26</sup>. Here again HM, is probably the most common; its intercalation results in the expansion of kaolinite *c*-lattice parameter, *c*-LP, from 7.2 to 10.3-10.4 Å<sup>26-28</sup>.

Here we report, for the first time, on the intercalation of Ti<sub>3</sub>C<sub>2</sub> with urea, HM, HM dissolved in DMF, and DMSO. The latter in turn enabled us to delaminate stacked Ti<sub>3</sub>C<sub>2</sub> layers into separate 2D MXene sheets. HM also intercalated Ti<sub>3</sub>CN and TiNbC.

A schematic of the intercalation of HM into MXene is shown in Fig. 1a. X-ray diffraction (XRD) showed that after intercalation with HM and/or DMF, the (0001) peaks were still present, but shifted to lower 2θ angles (Figs. 1b,c and Supplementary Fig. S1). Table 1 summarizes the *c*-LP values for Ti<sub>3</sub>C<sub>2</sub> treated with HM and HM in DMF. The initial *c*-LP was 19.5±0.1 Å, a value that does not change much with post-intercalation drying (Table 1). After exposure to HM or HM in DMF at 80 °C for 24 h, the *c*-LPs increased to 25.48±0.02 Å and 26.8±0.1 Å, respectively. The larger *c*-LP increase in the latter case points to a synergistic effect when HM is dissolved in DMF prior to its intercalation.

When the HM intercalated powders were heated to 120 °C in a vacuum oven, the *c*-LPs decreased from 25.48±0.02 to 20.6±0.3 Å, signifying that the intercalation process is essentially reversible. Heating powders intercalated with HM *and* DMF under the same conditions resulted in small increases in the 2θ angles (Fig. 1b-ii, c-ii). Thus, the HM/DMF combination is more resistant to de-intercalation than HM alone, possibly because of the higher boiling point of DMF (153 °C) compared to that of HM (114 °C). When the latter powder was vacuum dried at 200 °C, however, the *c*-LP decreased to 20.1±0.5 Å.

X-Ray photoelectron spectroscopy (XPS) (Supplementary Fig. S2) provides further evidence of intercalation. As previously reported<sup>17</sup>, exfoliated  $\text{Ti}_3\text{C}_2$  showed presence of Ti–C and Ti–O bonds as well as OH groups suggested by the presence of a O1s peak around 530 eV. A N1s signal was also observed around 400 eV in XPS spectra of  $\text{Ti}_3\text{C}_2$  treated with HM and HM/DMF (insets in Supplementary Figs. S2a and b, respectively). No nitrogen peaks were detected in  $\text{Ti}_3\text{C}_2$  prior to intercalation.

Scanning Electron Microscopy (SEM) images of  $\text{Ti}_3\text{C}_2$ , before and after HM treatment in DMF at 80 °C for 24 h, shown in Figs. 2a and b, respectively, confirm that: i) the MXene remain exfoliated after intercalation, and, ii) the layers thicken (Fig. 2b) apparently by gluing monolayers together forming 20-50 nm thick lamellas. Note that the absence of XRD peaks corresponding to a *c*-LP of 19.5 Å (Fig. 1b-i, 1c-i) implies that intercalation was complete.

Transmission electron microscopy (TEM) images and corresponding selected area electron diffraction (SAED) patterns of  $\text{Ti}_3\text{C}_2$  intercalated with HM in DMF at 80 °C for 24 h (Fig. 2e, f) showed that the basal planes' hexagonal structure remains unchanged (compare inset in Fig. 2d with Fig. 2f) after intercalation<sup>17</sup>. The intercalated interplanar spacing - 2.648 Å for (0 $\bar{1}$ 10) and 1.540 Å for (1 $\bar{2}$ 10) - result in an *a*-LP of 3.057 Å, in excellent agreement with the *a*-LP of  $\text{Ti}_3\text{C}_2$  before intercalation and that of the  $\text{Ti}_3\text{AlC}_2$ , *viz.* 3.058 Å<sup>17</sup>.

To demonstrate that intercalation is a general phenomenon rather than the exclusive property of  $\text{Ti}_3\text{C}_2$ ,  $\text{Ti}_3\text{CN}$  and  $\text{TiNbC}$  were also treated with HM. Similar to  $\text{Ti}_3\text{C}_2$ , the shift of the major XRD peak of these MXenes to lower  $2\theta$  values (Supplementary Fig. S3) confirmed their intercalation. It is thus reasonable to conclude that MXenes – like other layered materials - can be readily intercalated by a host of compounds.

To further our understanding, molecular dynamics (MD) calculations of  $\text{N}_2\text{H}_4$  inserted between OH-terminated  $\text{Ti}_3\text{C}_2$  layers were carried out (Fig. 3a). MXene supercells ( $4 \times 2 \times 1$  (a x b x c)) with different  $\text{N}_2\text{H}_4$  concentrations uniformly spaced between the MXene layers were constructed (see details in Supporting Information). With no  $\text{N}_2\text{H}_4$  molecules, the MD computed *c*-LP value is reasonably close to the experimental result (Table 1) and DFT calculated values<sup>17</sup>. When two  $\text{N}_2\text{H}_4$  molecules are introduced (one into each interlayer space), the *c*-LP sharply jumps to  $24.93 \pm 0.01$  Å (Fig. 3a). Further increase of the number of  $\text{N}_2\text{H}_4$  molecules results in only slightly changed *c*-LPs (from 24.93 to 25.31 Å), corresponding to a monolayer formation (Fig. 3a) within the widened interlayer MXene space. With 6  $\text{N}_2\text{H}_4$  molecules per supercell (3 inside each interlayer space as shown in Fig. 3b) the intercalant monolayer is complete and the introduction of the next pair of  $\text{N}_2\text{H}_4$  molecules results in a sharp increase of *c*-LP from  $25.31 \pm 0.04$  Å (6  $\text{N}_2\text{H}_4$  molecules) to  $27.28 \pm 0.03$  Å (8  $\text{N}_2\text{H}_4$  molecules) as shown in Fig. 3a, which is evidence for the onset of the formation of a second intercalant layer, (see also MD snapshot in Supplementary Fig. S4a).

The experimental *c*-LP value for  $\text{N}_2\text{H}_4$  intercalated MXene ( $c = 25.48$  Å, Table 1) corresponds to a N/C ratio  $\sim 0.39$  (Fig. 3a), i.e., to the formation of a nearly complete monolayer of  $\text{N}_2\text{H}_4$  molecules in each MXene interlayer space. The N/C ratio, determined by XPS for the HM intercalated MXene dried at room temperature, is 0.37, a very good agreement with the value deduced from the MD simulations ( $\sim 0.4$ ) for the situation with a nearly complete monolayer of  $\text{N}_2\text{H}_4$  molecules (Fig. 3b). Furthermore, the computed XRD pattern for the system of this composition is close to the one measured experimentally (Fig. 3c).

We also tried to intercalate thiophene, ethanol, acetone, tetrahydrofuran, formaldehyde, chloroform, toluene, hexane, DMF, DMSO, and urea into  $\text{Ti}_3\text{C}_2$  at room temperature. Of these, only DMSO and urea resulted in an increase in the *c*-LPs from  $19.5 \pm 0.1$  Å to  $35.04 \pm 0.02$  Å and

25.00±0.02 Å, respectively (Supplementary Fig. S5). It follows that DMF only intercalates into Ti<sub>3</sub>C<sub>2</sub> in the presence of HM. Coincidentally or not, of the aforementioned list, only DMSO and urea intercalate kaolinite<sup>26, 29</sup>.

XRD patterns, taken 3 weeks after the initial DMSO intercalation (Supplementary Fig. S5-ii, red curve), showed an even larger downshift of the (0002) peak positions corresponding to a *c*-LP of 44.8±0.1 Å. Based upon this result, combined with the observation that DMSO intercalated MXene powders are highly hygroscopic and become increasingly wet when stored in air over a few weeks, it is reasonable to assume that, over time, co-intercalation capillary condensation of water from ambient air into the interlayer space, occurred.

This discovery, in turn, was exploited to fully exfoliate – what we term delaminate herein (see Supplementary Fig. S6 for schematic) – Ti<sub>3</sub>C<sub>2</sub> sheets. After a weak sonication of DMSO intercalated MXene dispersed in deionized water, fully delaminated Ti<sub>3</sub>C<sub>2</sub> flakes were obtained. Centrifuged aqueous colloidal solutions of delaminated MXene flakes were quite stable. The majority of flakes were small, with a relatively narrow size distribution (Fig. 4a). Its colloidal nature was also confirmed by the observation of the Tyndall scattering effect by passing a red laser beam through the solution (inset Fig. 4a). SEM images clearly showed thin, electron-beam transparent, single MXene flakes precipitated from a drop of colloidal solution placed on a porous alumina membrane surface (Fig. 4b).

Binder-free MXene paper (inset Fig. 4d) was produced by filtering the aforementioned colloidal solution through a membrane (see Supporting Information). XRD patterns of the resulting “paper” (Fig. 4c) clearly showed that the non-basal peaks at ~ 60° 2 θ, *vanished*, after delamination. This result provides compelling evidence for the loss of order along all but the (0001) direction and consequently, full delamination.

A recent computational study<sup>24</sup>, concluded that delaminated  $\text{Ti}_3\text{C}_2$  layers would be attractive for Li ion battery anodes. To date, our Li-ion work was carried out on stacked multilayer particles<sup>22, 23</sup>. The breakthrough presented herein, however, allowed us to measure Li ion uptake on delaminated  $\text{Ti}_3\text{C}_2$  “paper”. As shown in Fig. 4d, the capacity of the latter is a factor of 4 higher than that of as-synthesized MXene. The “paper” showed a capacity of  $410 \text{ mAhg}^{-1}$  at a 1C cycling rate and  $110 \text{ mAhg}^{-1}$  at 36 C (Fig. 4d). The results shown in Fig. 4d are noteworthy since they show high Li capacities and a much better cyclabilities at high rates than graphite, used in commercial LIBs<sup>30</sup>.

In ways reminiscent of graphite and clays, MXenes can be intercalated by a variety of molecules. This discovery can lead to the intercalation of a broad range of organics and salts, as well as provide routes to carry out complex chemical reactions – such as catalysis, polymerization (similar to intercalated graphite)<sup>31</sup>, etc. – within the MXene interlayer galleries. Furthermore, the intercalation of DMSO between  $\text{Ti}_3\text{C}_2$  sheets, followed by sonication, resulted in their delamination into separate sheets in an aqueous suspension from which a  $\text{Ti}_3\text{C}_2$ -based “paper” was made. The Li uptake of the latter was significantly higher than its non-delaminated counterpart.

The results obtained herein are of both fundamental and practical importance. On the fundamental side, they establish MXenes as full-fledged members of the growing family of 2D materials, with all the potential that such materials provide. It is crucial to note, that in sharp contradistinction of all 2D materials made to date in which weakly bonded layers were exfoliated/delaminated, the work presented here was carried out on the MAX phases – that are layered - but in which the bonding is exceptionally *strong*. Said otherwise, the world of 2D solids need not be restricted to layered solids with weak bonds, which is truly paradigm shifting. From a practical point of view, our results open avenues for the development of numerous applications in composites, catalysis, sorption, and energy storage systems.

## Methods

**Intercalation of MXene.** To intercalate MXene with HM, the MXene powders were suspended either in HM or a 1:3 mixture of HM and DMF, and stirred for 24 h with a magnetic stirrer, either at room temperature, RT, or at 80 °C. In all cases, the weight ratio of HM:MXene was 10:1. When the treatment involved only HM, the suspensions were filtered and washed with ethanol. In case of intercalation with HM/DMF mixture, DMF was used for washing instead of ethanol. The powders were then dried in a desiccator under vacuum ( $< 10$  Torr) at RT for 24 h or in the vacuum oven ( $\sim 10^{-2}$  Torr) at 120 °C for 24 h.

Other organic compounds were also tried for intercalation into MXene. Those included DMSO, urea, DMF, acetone, ethyl alcohol, THF, chloroform, toluene, thiophene, and formaldehyde. In all cases the intercalation procedure was the same: i) 0.3 g of  $\text{Ti}_3\text{C}_2$  were mixed with 5 ml of each of the organic compounds listed above (excluding urea), then stirred for 24 h at RT; ii) in the case of urea, 5 ml of 50 wt.% aqueous solution of urea was added to 0.3 g of  $\text{Ti}_3\text{C}_2$  and stirred for 24 h at 60 °C. Afterwards, the resulting colloidal solutions were filtered and dried in a desiccator under vacuum ( $< 10$  Torr) at RT. A detailed experimental section (materials used, techniques of material preparation and de-intercalation of MXenes) can be found in the Supplementary Information.

**Delamination of MXene.** For delamination, DMSO was used. After stirring of  $\text{Ti}_3\text{C}_2$  with DMSO for 18 h at room temperature, the colloidal suspension was centrifuged to separate the intercalated powder from the liquid DMSO. After decantation of supernatant, deionized water was added to the residue in a volume ratio of MXene to water of 1:10. After bath sonication of the suspension for 6 h, the powder was filtered using a porous anodic aluminum oxide membrane filter (47 mm diameter, 0.2  $\mu\text{m}$  pore size, Whatman Anodisc) and dried in the oven at  $\sim 70$  °C overnight, resulting in MXene paper.



**Physical characterization.** XRD patterns were recorded with a powder diffractometer (Siemens D500, Germany) using Cu K $\alpha$  radiation ( $\lambda \sim 1.54 \text{ \AA}$ ) with  $0.02^\circ$   $2\theta$  steps and 1 s dwelling time. A SEM (Zeiss Supra 50VP, Germany) was used to obtain images of the particles. The 2D sheets were also imaged with a TEM (JEOL JEM-2100, Japan) using an accelerating voltage of 200 kV. The TEM samples were prepared by suspending the powders in isopropanol, sonicating for 1 min, and drying a drop of the mixture transferred on a 200 mesh lacey-carbon-coated copper grid. An XPS (PHI 5000, ULVAC-PHI, Inc., Japan) was used to analyze the surface elemental composition of the powders before and after intercalation. More information on techniques used for material characterization can be found in the Supplementary Information.

**Electrochemical characterization.** Electrochemical measurements were carried out using coin cells (see Supplementary Information). The lithium ion batteries' cyclabilities were studied using a galvanostatic charge-discharge cycling (GV) and a battery cycler (Arbin BT-2143-11U, College Station, TX, USA). In GV tests, the batteries were charged and discharged between 0 and 2.5 V vs. Li/Li $^+$  with an imposed current, while the potential change was measured. From this measurement, the specific capacities were calculated for each cycle as  $C = I \times t / m$  where  $C$  is the specific capacitance (in mAh.g $^{-1}$ ),  $I$  is the current (in mA),  $t$  is the time (in h) and  $m$  is the mass of active material (in g). Note that for the MXene-based electrode before delamination, only the MXene mass without that of the additives, was taken into account. For the delaminated MXene, since there were no additives, the mass considered that of the MXene film.

## References

1. Dresselhaus, M.S. & Dresselhaus, G. Intercalation compounds of graphite. *Adv. Phys.* **30**, 139-326 (1981).

2. Pinnavaia, T.J. Intercalated clay catalysts. *Science* **220**, 365-371 (1983).
3. Ogawa, M. & Kuroda, K. Photofunctions of intercalation compounds. *Chem. Rev.* **95**, 399-438 (1995).
4. Podsiadlo, P., *et al.* Ultrastrong and stiff layered polymer nanocomposites. *Science* **318**, 80-83 (2007).
5. Ma, R.Z. & Sasaki, T. Nanosheets of oxides and hydroxides: Ultimate 2D charge-bearing functional crystallites. *Adv. Mater.* **22**, 5082-5104 (2010).
6. McKelvy, M.J. & Glaunsinger, W.S. Molecular intercalation reactions in lamellar compounds. *Annu. Rev. Mater. Sci.* **41**, 497-523 (1990).
7. Novoselov, K.S., *et al.* Two-dimensional atomic crystals. *P. Natl. Acad. Sci. USA* **102**, 10451-10453 (2005).
8. Stoller, M.D., Park, S., Zhu, Y., An, J. & Ruoff, R.S. Graphene-based ultracapacitors. *Nano Lett.* **8**, 3498-3502 (2008).
9. Shih, C.J., *et al.* Bi- and trilayer graphene solutions. *Nat. Nanotechnol.* **6**, 439-445 (2011).
10. Eda, G. & Chhowalla, M. Chemically derived graphene oxide: Towards large-area thin-film electronics and optoelectronics. *Adv. Mater.* **22**, 2392-2415 (2010).
11. Kumar, A., *et al.* Direct synthesis of lithium-intercalated graphene for electrochemical energy storage application. *ACS Nano* **5**, 4345-4349 (2011).
12. Coleman, J.N., *et al.* Two-dimensional nanosheets produced by liquid exfoliation of layered materials. *Science* **331**, 568-571 (2011).
13. Zhang, Z., Liu, X., Yakobson, B.I. & Guo, W. Two-dimensional tetragonal TiC monolayer sheet and nanoribbons. *J. Am. Chem. Soc.* **134**, 19326-19329 (2012).
14. Terrones, M. Materials science: Nanotubes unzipped. *Nature* **458**, 845-846 (2009).

15. Eda, G., *et al.* Photoluminescence from chemically exfoliated MoS<sub>2</sub>. *Nano Lett.* **11**, 5111-5116 (2011).
16. Barsoum, M.W. The M(N+1)AX(N) phases: A new class of solids; Thermodynamically stable nanolaminates. *Prog. Solid State Chem.* **28**, 201-281 (2000).
17. Naguib, M., *et al.* Two-dimensional nanocrystals produced by exfoliation of Ti<sub>3</sub>AlC<sub>2</sub>. *Adv. Mater.* **23**, 4248-4253 (2011).
18. Naguib, M., *et al.* Two-dimensional transition metal carbides. *ACS Nano* **6**, 1322-1331 (2012).
19. Viculis, L.M., Mack, J.J. & Kaner, R.B. A chemical route to carbon nanoscrolls. *Science* **299**, 1361-1361 (2003).
20. Savoskin, M.V., *et al.* Carbon nanoscrolls produced from acceptor-type graphite intercalation compounds. *Carbon* **45**, 2797-2800 (2007).
21. Enyashin, A.N. & Ivanovskii, A.L. Atomic structure, comparative stability and electronic properties of hydroxylated Ti<sub>2</sub>C and Ti<sub>3</sub>C<sub>2</sub> nanotubes. *Comput. Theor. Chem.* **989**, 27-32 (2012).
22. Naguib, M., *et al.* MXene: a promising transition metal carbide anode for lithium-ion batteries. *Electrochem. Commun.* **16**, 61-64 (2012).
23. Come, J., *et al.* A non-aqueous asymmetric cell with a Ti<sub>2</sub>C-based two-dimensional negative electrode. *J. Electrochem. Soc.* **159**, A1368-A1373 (2012).
24. Tang, Q., Zhou, Z. & Shen, P.W. Are MXenes promising anode materials for Li ion batteries? Computational studies on electronic properties and Li storage capability of Ti<sub>3</sub>C<sub>2</sub> and Ti<sub>3</sub>C<sub>2</sub>X<sub>2</sub> (X = F, OH) monolayer. *J. Am. Chem. Soc.* **134**, 16909-16916 (2012).
25. Park, S., *et al.* Colloidal suspensions of highly reduced graphene oxide in a wide variety of organic solvents. *Nano Lett.* **9**, 1593-1597 (2009).

26. Ledoux, R.L. & White, J.L. Infrared studies of hydrogen bonding interaction between kaolinite surfaces and intercalated potassium acetate, hydrazine, formamide, and urea. *J. Colloid. Interf. Sci.* **21**, 127-152 (1966).
27. Frost, R.L., Kristof, J., Horvath, E., Martens, W.N. & Klopogge, J.T. Complexity of intercalation of hydrazine into kaolinite - A controlled rate thermal analysis and DRIFT spectroscopic study. *J. Colloid. Interf. Sci.* **251**, 350-359 (2002).
28. Deng, Y.J., Dixon, J.B. & White, G.N. Molecular configurations and orientations of hydrazine between structural layers of kaolinite. *J. Colloid. Interf. Sci.* **257**, 208-227 (2003).
29. Olejnik, S., Aylmore, L.A.G., Posner, A.M. & Quirk, J.P. Infrared spectra of kaolin mineral-dimethyl sulfoxide complexes. *J. Phys. Chem.* **72**, 241-249 (1968).
30. Tran, T.D., Feikert, J.H., Pekala, R.W. & Kinoshita, K. Rate effect on lithium-ion graphite electrode performance. *J. Appl. Electrochem.* **26**, 1161-1167 (1996).
31. Shioyama, H. & Akita, T. A new route to carbon nanotubes. *Carbon* **41**, 179-181 (2003).

### **Acknowledgements**

We thank Maria Lukatskaya for an SEM image, Boris Dyatkin for help with sample preparation and BET analysis, Laura Allen for help in making the MXene paper, and the Centralized Research Facility of Drexel University for providing access to XRD, XPS, SEM, and TEM. This work was funded by the Assistant Secretary for Energy Efficiency and Renewable Energy, Office of Vehicle Technologies of the U.S. Department of Energy under Contract No. DE-AC02-05CH11231, Subcontract 6951370 under the Batteries for Advanced Transportation Technologies (BATT) Program.

### **Author contributions**

O.M. carried out all of the intercalation work and characterization by TEM and part of XRD analysis. M.N. carried out synthesis of pure MAX phase and MXene material, all of the delamination work and characterization by the XRD and SEM. Y.D. and M.N. performed electrochemical measurements. V.M. performed the computational studies and overseen the experimental program. Y.G. and M.W.B. conceived and directed the project. The manuscript was prepared by O.M., V.M., M.N., M.W.B. and Y.G. All authors discussed the results and commented on the manuscript.

### **Additional information**

Supplementary information is available in the online version of the paper. Reprints and permission information is available online at <http://www.nature.com/reprints>. Correspondence and requests for materials should be addressed to Y.G. or M.W.B.

### **Competing financial interest**

The authors declare no competing financial interests.

Figure

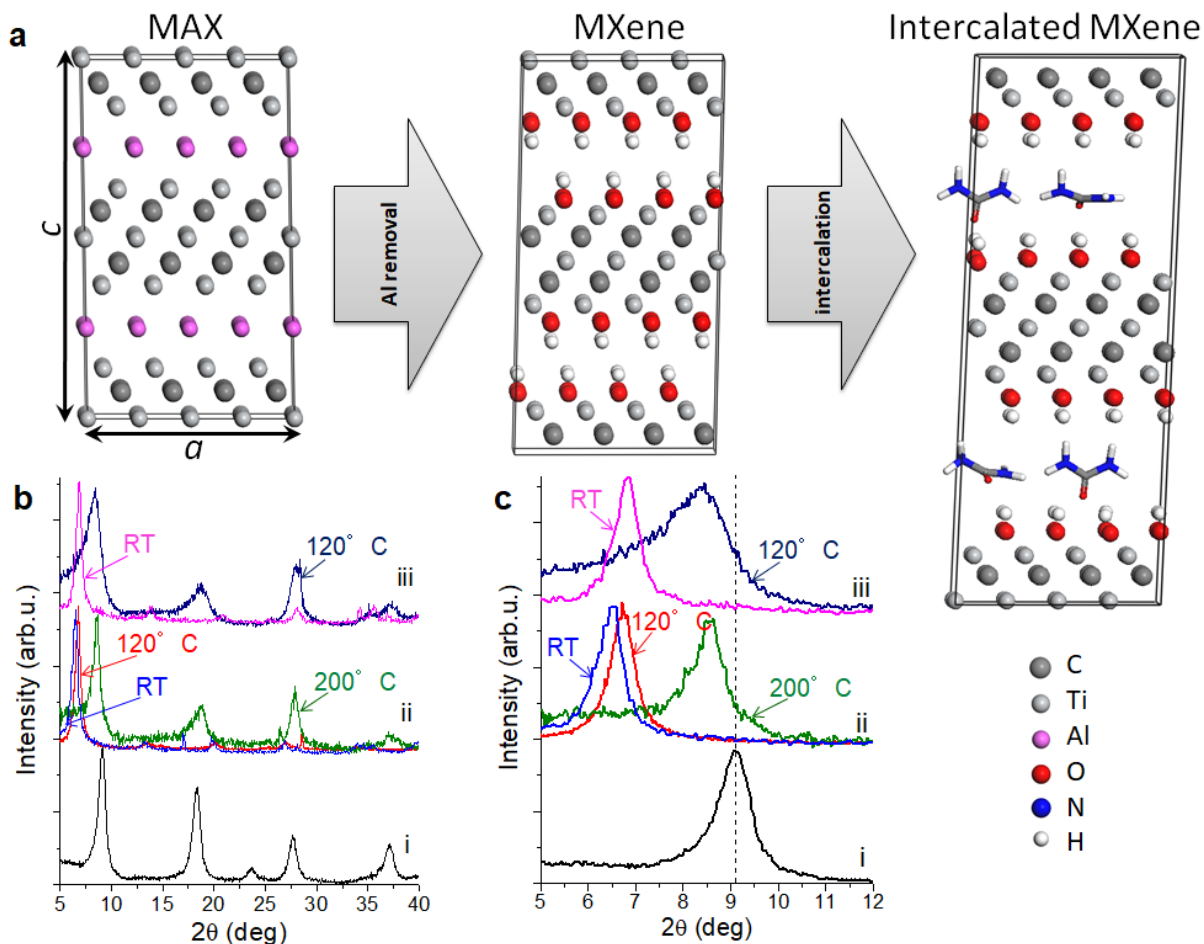


**Figure 1 | Evidence of MXene intercalation.** **a**, Schematic of synthesis and intercalation of Ti<sub>3</sub>C<sub>2</sub>. First, the Al layer is removed from the corresponding MAX phase in 50% aqueous HF. The MXene is then treated with an intercalant (urea is shown as an example) yielding intercalation compounds. **b**, XRD patterns of Ti<sub>3</sub>C<sub>2</sub>: i) as-received, before any treatment, ii) after HM in DMF treatment, washed with DMF, iii) after HM treatment, washed with ethanol, and dried at different conditions. **c**, Zoom-ins of (b) in the 5-12° 2θ range showing (0002) peaks.

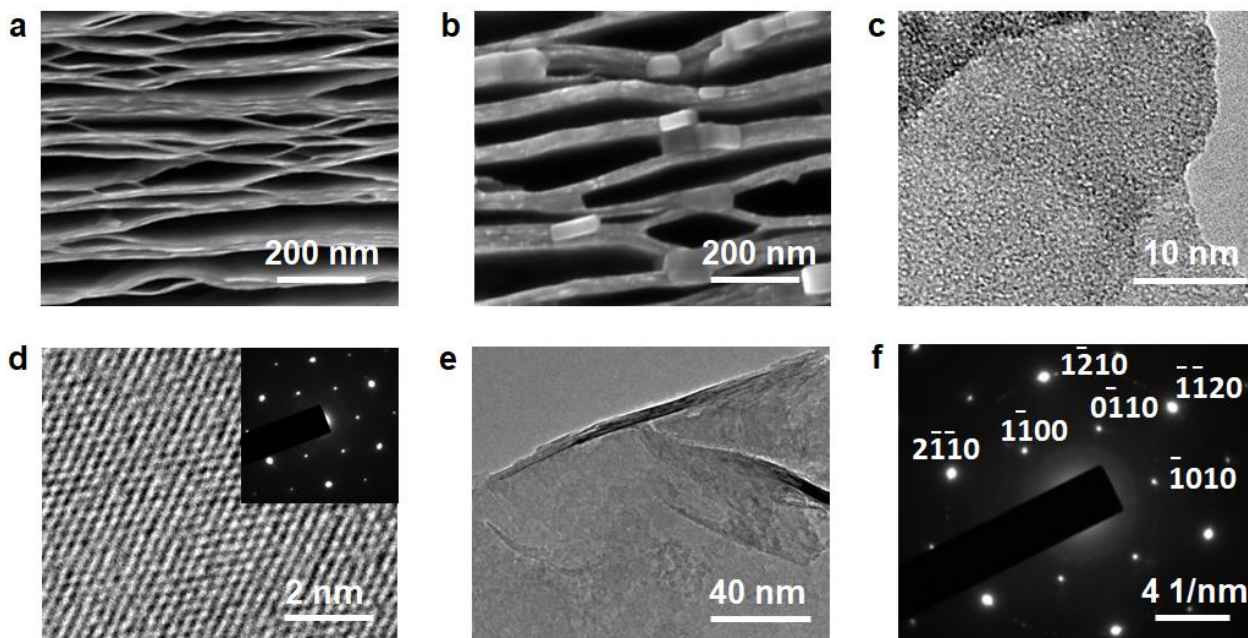


**Figure 2 | Morphology characterization.** **a,b**, SEM images before **(a)** and after **(b)** intercalation of  $\text{Ti}_3\text{C}_2$  with HM and DMF (24 h at 80 °C), respectively. **c,d**, TEM **(c)** and HRTEM **(d)** images (inset shows SAED pattern) before intercalation. **e,f**, TEM image **(e)** and SAED pattern **(f)** of intercalated  $\text{Ti}_3\text{C}_2$ .

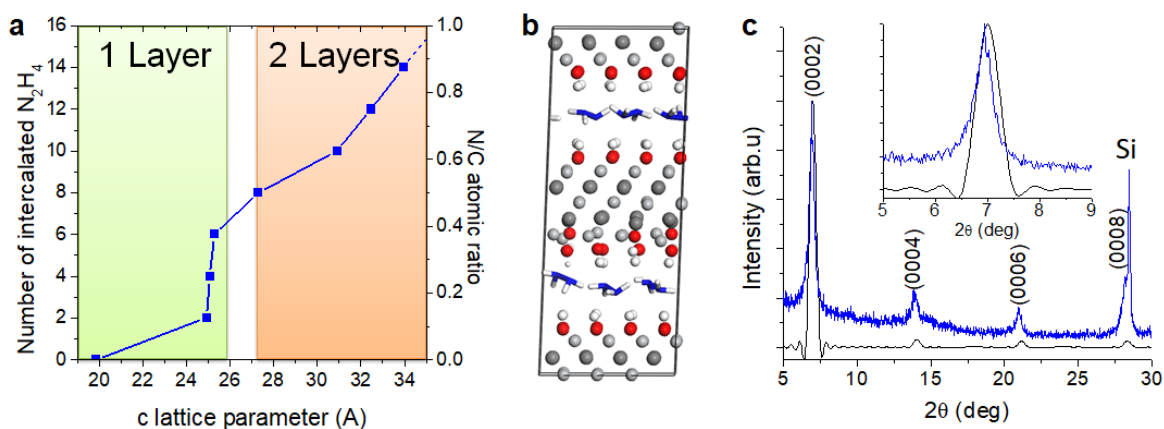


**Figure 3 | MD simulations of OH-terminated  $\text{Ti}_3\text{C}_2$  intercalated with  $\text{N}_2\text{H}_4$ .** **a**, Change in MXene  $c$ -LP as a function of the number of  $\text{N}_2\text{H}_4$  intercalated molecules. As the latter is increased, first a

monolayer of  $N_2H_4$  molecules is formed, corresponding to the N/C ratio  $\sim 0.4$  ( $c = 25\text{-}26 \text{ \AA}$ ). Further increase in results in onset of the second layer formation, which is not complete up to the maximum N/C ratio employed in the simulations (N/C = 0.875). **b**, MD snapshot of MXene for N/C ratio 0.375 (6  $N_2H_4$  per a  $4 \times 2 \times 1$  MXene supercell) showing near complete  $N_2H_4$  monolayer. **c**, Comparison of simulated (black) and experimental XRD patterns (blue).

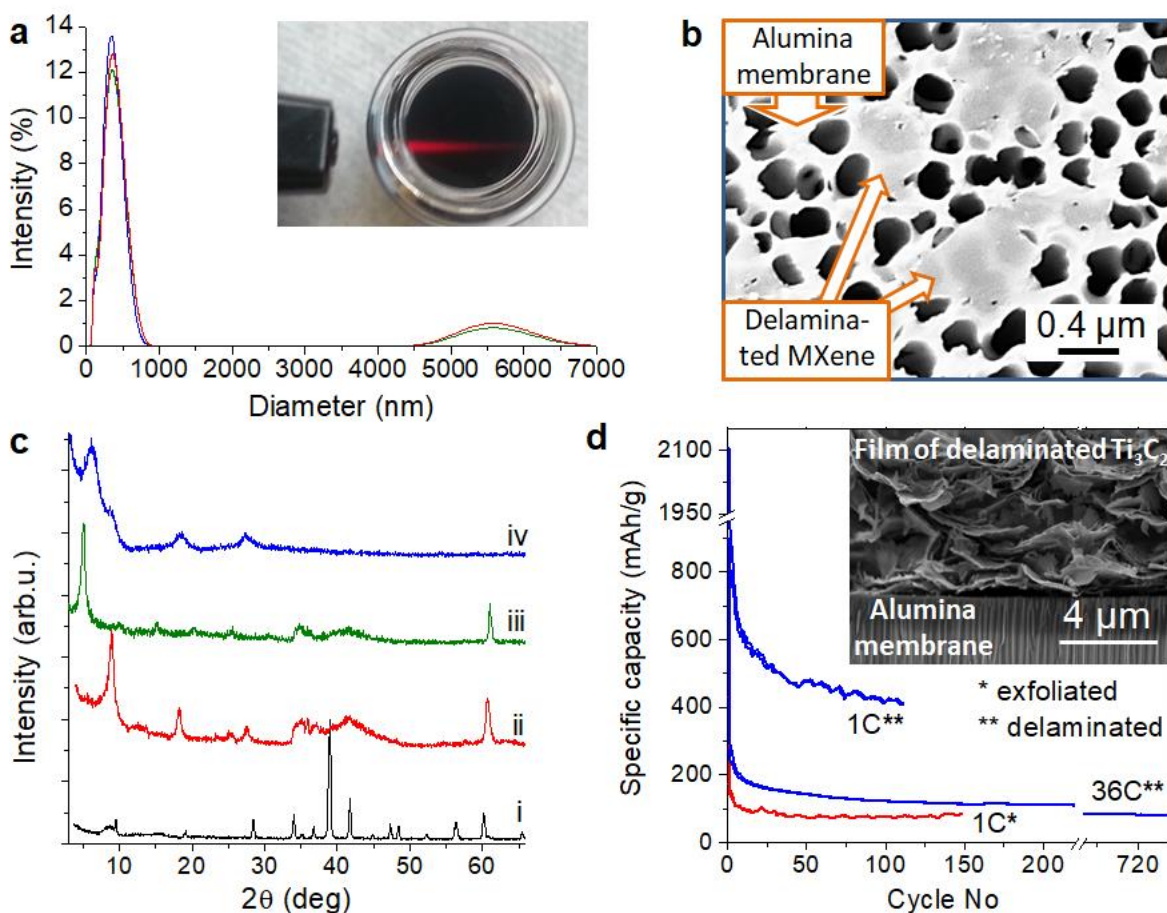


**Figure 4 | Delaminated  $Ti_3C_2$  and its properties.** **a**, Particle size distribution in aqueous colloidal solution; Inset shows Tyndall scattering effect of solution. **b**, SEM images of  $Ti_3C_2$  flakes on the alumina membrane. **c**, XRD patterns of, (i)  $Ti_3AlC_2$ , (ii) exfoliated, (iii) DMSO intercalated and (iv)



delaminated  $\text{Ti}_3\text{C}_2$ . Note disappearance of peak at  $60^\circ$ . **d**, Comparison of performance of exfoliated and delaminated  $\text{Ti}_3\text{C}_2$  as anode material in Li-ion batteries. Inset shows SEM image of an *additive-free* film of delaminated  $\text{Ti}_3\text{C}_2$  filtered through the membrane.

**Table 1.** *c* lattice parameters, in Å, for non-intercalated Ti<sub>3</sub>C<sub>2</sub> and Ti<sub>3</sub>C<sub>2</sub> powders treated with HM, HM and DMF, and dried in different conditions.

<b>Intercalant</b>	Non-intercalated	MD – non-intercalated	HM (XRD) <sup>‡</sup>	MD (N/C ratio 0.375)	HM in DMF (XRD) <sup>‡</sup>
Initial material*	19.5±0.1	19.85±0.01	25.48±0.02	25.31±0.04	26.8±0.1
After drying @ 120 °C	19.5±0.1	N/A	20.6±0.3	N/A	26.0± 0.2
Vacuum drying @ 200°C	19.3±0.2	N/A	N/A	N/A	20.1± 0.5

\* Prior to intercalation, the Ti<sub>3</sub>C<sub>2</sub> powder was dried in a desiccator under vacuum (< 10 Torr) at room temperature for 24 h.

<sup>‡</sup> Both HM and HM in DMF treatments were carried out at 80 °C for 24 h (see details in Supporting Information).